RESEARCH ARTICLE

Comparative evaluation of polynomial and Lorentzian lineshape-fitted amine CEST imaging in acute ischemic stroke

Jing Cui[1,2] 🆔 | Aqeela Afzal[3] | Zhongliang Zu[1,2] 🆔

[1]Vanderbilt University Institute of Imaging Science, Vanderbilt University Medical Center, Nashville, Tennessee, USA

[2]Department of Radiology and Radiological Sciences, Vanderbilt University Medical Center, Nashville, Tennessee, USA

[3]Department of Neurological Surgery, Vanderbilt University Medical Center, Nashville, Tennessee, USA

Correspondence
Zhongliang Zu, Vanderbilt University
Institute of Imaging Science, 1161 21st
Ave. S, Medical Center North, AAA-3112,
Nashville, TN 37232-2310, USA.
Email: zhongliang.zu@vumc.org

Purpose: Chemical exchange saturation transfer signals from amines are sensitive to pH, and detection of these signals can serve as an alternative pH imaging method to amide proton transfer (APT). However, conflicting results regarding amine CEST imaging at 2 ppm in ischemic stroke have been reported. Here, we correlated amine CEST with APT in animal stroke models to evaluate its specificity to pH, and investigated the reason for the different results through simulations and sample studies.

Methods: A three-point quantification method was used to quantify APT. A polynomial fit method and a multiple-pool Lorentzian fit method were used to quantify amine CEST. Samples of creatine and glutamate were prepared to study the different CEST effects from arginine amine and fast exchanging pools. Samples of tissue homogenates with different pH were prepared to study the variation in CEST signals due only to changes in pH.

Results: The polynomial fit of amine CEST at 2 ppm had a significant correlation with APT, whereas the Lorentzian fit did not. Further studies showed that arginine amine contributed to the polynomial fit, whereas both the arginine amine and the fast exchanging pools contributed to the Lorentzian fit with their CEST effects varying in opposite directions after stroke. The CEST signal from the fast exchanging pool decreased, probably due to the reduced pool concentration but not pH.

Conclusion: The variation in opposite directions led to an insignificant correlation of the Lorentzian fit of amine CEST with APT and the different results in different experimental conditions.

KEYWORDS
amide proton transfer, amine, chemical exchange saturation transfer, Lorentzian fit, polynomial fit

1 | INTRODUCTION

Tissue acidosis is associated with altered cellular metabolism in various diseases, such as ischemic stroke. During ischemia, anaerobic respiration is initiated and the production of lactate often causes tissue acidosis, thus decreasing intracellular pH. Recent studies show that pH-weighted imaging can provide better delineation of salvageable ischemic tissue than the diffusion-perfusion mismatch.[1,2] Therefore, noninvasive in vivo pH MRI techniques are very important for stroke diagnosis. Phosphorus MRS (^{31}P-MRS) and lactate MRS have been applied to detect pH in vivo. However, these methods are limited by their low SNRs, resulting in low spatial and temporal resolution. Chemical exchange saturation transfer is an emerging MR contrast mechanism that is sensitive to both the solute molecular concentration and the solute-water exchange rate. This exchange rate depends on pH; thus, CEST has potential as a method to measure pH changes in ischemic tissue. Because CEST indirectly detects the solute-water exchange effect by measuring the change in the water signal due to an accumulative exchange effect between the saturated solute molecular protons and water protons, it has high detection sensitivity.

Amide proton transfer (APT) imaging is a variation of the CEST technique, which originates from the chemical exchange between water protons and amide protons on the backbone of mobile proteins/peptides at approximately 3.5 ppm from water.[3] Previously, APT was successfully applied to detect ischemic stroke[4] and has been shown to have a significant association with tissue lactic acidosis during acute ischemic stroke.[5] The drawback of APT is that it has "negative contrast" in the stroke lesion, which may make it difficult to distinguish from imaging artifacts. Amines are another major exchange pool in biological tissues. Previous reports have shown that there are arginine amines at approximately 2 ppm from creatine and proteins[6,7] and lysine amines at approximately 3 ppm from glutamate and proteins.[8,9] Arginine amines have an exchange rate of several hundred Hertz,[10-13] which is in the intermediate exchange regime, and lysine amines have an exchange rate of several thousand Hertz,[8] which is in the fast exchange regime; both of these are much faster than the amide-water exchange rate of about 30 s^{−1}.[4] By choosing appropriate RF saturation powers, the CEST signal from arginine amines could be higher than APT and could also demonstrate "positive contrast" in the stroke lesion. Because the arginine amine CEST effect at 2 ppm has a narrow peak that can be clearly observed on the CEST Z-spectrum acquired with relatively low RF saturation powers (eg, 1 μT), this type of transfer has drawn attention in the past few years.[14-17]

However, although amine CEST imaging shows promise in detecting pH, there are challenges to its widespread use. First, the dependence of amine CEST on pH is complex, as the concentration of metabolites that contribute to the effects of amine CEST, such as glutamate, glutamine, creatine and phosphocreatine, change significantly in acute stroke[18]; second, the specific quantification of the amine CEST effect is difficult, as the CEST peaks from amines, especially those from fast exchanging amines, are broad and thus may overlap with others. Previously, the arginine amine CEST effect at approximately 2 ppm was quantified by a polynomial fit method[7,19] and a multiple-pool Lorentzian lineshape fit method.[10,14,15,17] However, whether these methods are specific to the pH variation in ischemic stroke has not been evaluated.

On a CEST Z-spectrum acquired with relatively low RF saturation powers, CEST effects from amides at approximately 3.5 ppm, amines at approximately 2 ppm, nuclear Overhauser enhancement (NOE) at approximately −1.6 ppm (NOE[−1.6]), NOE at approximately −3.5 ppm (NOE[−3.5]), and semisolid magnetization transfer (MT) at approximately −2.3 ppm[20] can be observed.[21] Previously, we performed a five-pool (amide, amine, water, NOE[−1.6], and NOE[−3.5]) model Lorentzian lineshape fit of CEST signals from animal stroke models acquired with a saturation power (ω_1) of 1 μT at 7T MRI, and found that the fitted amine CEST effect at 2 ppm was not significantly different between the stroke lesion and the contralateral normal tissue (the semisolid MT effect was removed by subtracting signals at 5 ppm before the Lorentzian fit in this method).[15] Wu et al[14] performed another type of five-pool (amide, amine, water, NOE[−3.5], and semisolid MT) model fit of CEST signals from animal stroke models acquired with ω_1 of 1.5 and 0.75 μT at 4.7T MRI, and found that the fitted amine CEST effect at 2 ppm decreased significantly in the stroke lesion. Tee et al[17] have performed a six-pool (amide, amine, water, NOE[−1.6], NOE[−3.5], and semisolid MT) model fit of CEST signals from animal stroke models acquired with an averaged ω_1 of 0.8 μT at 9.4T MRI, and found that the fitted amine CEST effect at 2 ppm increased significantly in the stroke lesion. These different results, obtained under different experimental conditions, may suggest the complex signal origin of amine CEST imaging.

In this paper, we applied the polynomial fit method and the multiple-pool Lorentzian lineshape fit method to quantify the arginine amine CEST effect at 2 ppm in an acute ischemic stroke model, evaluated the specificity of these methods to pH by correlating their results with those of APT, and studied their contrast origin through numerical simulations and experiments on samples of metabolites with different exchange pools and sample of tissue homogenates with different pH values.

2 | METHODS

2.1 | Three-point quantification of APT

The three-point quantification method uses the subtraction of a CEST signal acquired with RF saturation pulses at the resonance frequency of amide and an average of two CEST signals acquired at two nearby frequency offsets.[22,23] Compared with other APT quantification methods,[4,24] the three-point method has less influence from other pools, especially at high field strengths and under low RF saturation powers where the CEST dips from other pools are far from those of the APT on the CEST Z-spectrum. Here, we assume that the three-point quantification of APT can specifically measure pH, and use it as a standard to compare with amine CEST imaging. The reference signal (S_{ref}) for the three-point quantification of APT was created by the straight line between two points at 3 ppm and 4 ppm and is defined by

$$S_{ref}(\Delta\omega) = S(3\text{ ppm}) + (S(4\text{ ppm}) - S(3\text{ ppm})) \cdot \frac{\Delta\omega - 3\text{ ppm}}{4\text{ ppm} - 3\text{ ppm}}$$

(1)

where $\Delta\omega$ is the RF saturation frequency offset from water.

2.2 | Multiple-pool Lorentzian lineshape fit of amine CEST at 2 ppm

Multiple-pool Lorentzian lineshape fitting of the Z-spectrum was performed using a nonlinear optimization algorithm. Equation 2 gives the model function of the Lorentzian fit method.

$$\frac{S(\Delta\omega)}{S_0} = 1 - \sum_{i=1}^{N} L_i(\Delta\omega)$$

(2)

Here, $L_i(\Delta\omega) = A_i/(1+(\Delta\omega-\Delta_i)^2/(0.5\ W_i)^2)$, which represents a Lorentzian line with central frequency offset from water (Δ_i), peak FWHM (W_i), and peak amplitude (A_i). The value of N is the number of fitted pools; S is the measured signal on the Z-spectrum; and S_0 is the nonirradiation control signal. A six-pool model Lorentzian fit including amide (L_1), amine (L_2), water (L_3), NOE(−1.6) (L_4), NOE(−3.5) (L_5), and semisolid MT (L_6) was performed to process the Z-spectra acquired from the animals. A five-pool model Lorentzian fit including L_1, L_2, L_3, L_5, and L_6 was performed to process the Z-spectra acquired from samples of tissue homogenates. The number of fitted pools was estimated by observing the CEST effects on the measured Z-spectra from the animals and samples. Table

TABLE 1 Starting points and boundaries of the amplitude, width, and offset of the six-pool Lorentzian fit

	Start	Lower	Upper
A_{water}	0.9	0.02	1
W_{water}	1.4	0.3	10
Δ_{water}	0	−1	1
A_{amide}	0.01	0	0.3
W_{amide}	0.5	0.4	3
Δ_{amide}	3.5	3	4
A_{amine}	0.01	0	0.3
W_{amine}	1.5	0.5	5
Δ_{amine}	2	1	3
$A_{NOE(-1.6)}$	0.01	0	0.3
$W_{NOE(-1.6)}$	1	0.5	1.5
$\Delta_{NOE(-1.6)}$	−1.6	−2	−1
$A_{NOE(-3.5)}$	0.01	0	0.3
$W_{NOE(-3.5)}$	3	1	5
$\Delta_{NOE(-3.5)}$	−3.5	−4.5	−2.5
A_{MT}	0.1	0	0.3
W_{MT}	25	10	100
Δ_{MT}	0	−4	4

Note: The unit of peak width and offset is parts per million (ppm).

1 lists the starting points and boundaries of the fits based on our experiences and previous publications.[21,25] The S_{ref} for quantifying the amine CEST effect was obtained by the sum of all Lorentzians, except that of the amine pool in Equation 2.[26] Equation 3 gives the model function of S_{ref} for the multiple-pool Lorentzian fit of amine CEST in the animal studies:

$$\frac{S_{ref}(\Delta\omega)}{S_0} = 1 - (L_1(\Delta\omega) + L_3(\Delta\omega) + L_4(\Delta\omega) + L_5(\Delta\omega) + L_6(\Delta\omega))$$

(3)

2.3 | Polynomial fit of amine CEST at 2 ppm

We used a third-order polynomial function to fit S_{ref} to the polynomial fit, as follows[7]:

$$\frac{S_{ref}(\Delta\omega)}{S_0} = C0 + C1(\Delta\omega - \Delta_{amine}) + C2(\Delta\omega - \Delta_{amine})^2 + C3(\Delta\omega - \Delta_{amine})^3$$

(4)

where Δ_{amine} is the amine resonance frequency offset, which is approximately 2 ppm. The values of C0-C3 are the zero-order to third-order polynomial coefficients. Here, we fitted

the background CEST signals from 1 ppm to 1.5 ppm and 2.5 ppm to 3 ppm to Equation 4, to obtain the S_{ref} for the polynomial fit of amine at 2 ppm. The order of the polynomial coefficients was chosen so that the polynomial could fit the *in vivo* background signals with sufficient accuracy, as shown in Supporting Figure S1.

2.4 | Inverse analysis to specifically quantify CEST effects

We used apparent exchange-dependent relaxation (AREX)[27] to specifically quantify the CEST effects.

$$AREX (\Delta\omega) = \left(\frac{S_0}{S(\Delta\omega)} - \frac{S_0}{S_{ref}(\Delta\omega)} \right) R_{1obs} (1 + f_m) \quad (5)$$

where R_{1obs} is the observed water longitudinal relaxation rate, and f_m is the semisolid pool concentration.[27] The term $(1+f_m)$, although is not shown in previous AREX imaging,[28] has been proved to be able to make the AREX more specific to chemical exchange effect.[27] The AREX metrics obtained with the three-point quantification (3pt), multiple-pool Lorentzian lineshape fit (mfit), and polynomial fit (poly) were termed $AREX_{3pt}$, $AREX_{mfit}$, and $AREX_{poly}$, respectively.

2.5 | Sample and animal preparation

Tissue homogenates were prepared by removing the brain from a freshly sacrificed healthy rat. The intact brain tissue was weighed and washed quickly in 1-time phosphate-buffered saline to remove residual blood. Then, after the addition of 4-times phosphate-buffered saline (wt/wt), the tissues were homogenized with a motor-driven blade-type homogenizer (Brinkmann Polytron PT3000; Kinematica, Malters, Switzerland) at max speed of approximately 23 000 rpm for 2 × 30 second bursts. The homogenates were divided into two aliquots, in which the pH was titrated to 7.1 and 6.7 at room temperature by using NaOH/HCl. The pH values of the two samples were measured with a pH meter before and after MRI measurements to ensure they were stable during the experiments. Two samples of metabolites, 6 mM creatine and 10 mM glutamate, were prepared in phosphate-buffered saline buffer. The pH was titrated to 7.0 for both samples. The creatine sample was used to study the characteristics of the CEST peak from the intermediate exchanging arginine amine. The glutamate sample was used to study the characteristics of the CEST peak from the fast exchanging pool. The MRI measurements on these samples of tissue homogenates and metabolites were performed at 37°C.

Ischemic stroke was induced through middle cerebral artery occlusion in the left hemispheres of five rat brains. First, the animals were anesthetized with 4% isoflurane in an induction chamber and maintained at 2%-2.5% isoflurane during surgery. Ophthalmic ointment was applied as a lubricant to both eyes before surgery, and a rectal temperature probe was used to maintain the animals' core temperature. Then, a 30-mm, silicon-coated, 4-0 nylon suture (Doccol, Redlands, CA) was routed into the left internal carotid artery and advanced until it occluded the middle cerebral artery at a depth of 18-20 mm. The suture was tightened around the filament, and the incision was closed. Immediately after surgery, the rats were taken from the surgery room to the MRI scanner. Animals were anesthetized with 2% isoflurane and 98% O$_2$, and the breathing rate was monitored throughout the experiments. The rat rectal temperature was maintained at approximately 37°C throughout the experiments by using a warm-air feedback system. All procedures were reviewed and approved by the Vanderbilt University Institutional Animal Care and Use Committee.

2.6 | Magnetic resonance imaging

Experiments were performed on a Varian DirectDrive horizontal 7T MRI with a 38-mm Doty RF coil (Doty Scientific, Columbia, SC) for the animal studies, and a Varian DirectDrive horizontal 9.4T MRI with a 38-mm Litz RF coil (Doty Scientific) for the sample studies. The CEST measurements were performed by applying a continuous-wave CEST sequence with an RF saturation length of 5 seconds and an ω_1 of 1 μT followed by single-shot spin-echo EPI on the animals, and with an RF saturation length of 8 seconds and an ω_1 of 1 μT followed by FID acquisition on all samples. (Because T_1 in the samples is longer than that in tissues, we used a longer RF saturation length to ensure that the exchanging spin system in the samples reaches steady state) Z-spectra were acquired with frequency offsets at ± 4000, ± 3500, ± 3000, ± 2500, and from -1500 to 1500 Hz with a step size of 50 Hz (-13.33 to 13.33 ppm on 7 T) on the animals, at ± 6500, ± 6000, ± 5500, ± 5000, ± 4500, ± 4000, ± 3500, and from -2000 to 2000 Hz with a step size of 50 Hz (-16.25 to 16.25 ppm on 9.4 T) on samples of tissue homogenates, and from -2000 to 2000 Hz with a step of 50 Hz (-5 to 5 ppm on 9.4 T) on samples of metabolites. Control signals were obtained by setting the RF offset to 100 000 Hz (333 ppm on 7 T and 250 ppm on 9.4 T). In the animal experiments, R_{1obs}, f_m, and the equilibrium longitudinal magnetization of the water pool (M_{0w}) were obtained using a selective inversion-recovery method with TIs of 4, 5, 6, 8, 10, 12, 15, 20, 50, 200, 500, 800, 1000, 2000, 4000, and 6000 ms.[29] The

inversion pulse affects the water pool and the semisolid pool to different degrees. After the inversion pulse, MT between these two pools will occur. The water signal recovery depends on both the MT effect and the longitudinal relaxation effect. At the beginning of the recovery, the MT effect takes the lead; after that, the longitudinal relaxation effect dominates. Thus, the water signal recovery has two different rates: a slow recovery rate for long TIs and a fast recovery rate for short TIs. By fitting the measured signals to a bi-exponential function of the inversion time, quantitative information on the MT effect and the longitudinal relaxation rate can be derived. In the sample experiments, R_{1obs} was obtained using an inversion-recovery sequence, and f_m was set to 0 because it was very small. (The tissue homogenate sample was diluted by 5 times, and its f_m was estimated to be about 0.02, assuming an average f_m of 0.1 in brain.) All images were acquired with a matrix size of 64×64, a FOV of 30×30 mm, and one average. Baseline and later images were acquired 1-3 days before and at 0.5-1 hour, 1-1.5 hours, and 1.5-2 hours after the middle cerebral artery occlusion surgery.

2.7 | Numerical simulations

Simulated CEST Z-spectra were first created using a two-pool (solute at 2 ppm and water at 0 ppm) model numerical simulation of Bloch-McConnell equations. The $AREX_{mfit}$ and $AREX_{poly}$ fit of amine at 2 ppm as a function of the exchange rate (k_{sw}) were then obtained by processing the simulated Z-spectra. Simulation parameters included $T_{1s} = 1.5$ seconds, $T_{2s} = 15$ ms, $T_{1w} = 1.5$ seconds, and $T_{2w} = 60$ ms, where the "s" and "w" subscripts correspond to solute and water, respectively. The solute concentration was 0.1% of water content. Sequence parameters including the RF saturation length and saturation frequency offsets were the same as those used in the animal experiments.

The simulation contains six Bloch-McConnell equations and can be written as $\frac{d\mathbf{M}}{dt} = \mathbf{AM} + \mathbf{M}_0$, where A is a 6×6 matrix. The water and solute pools each has three coupled equations representing their x, y, and z components. Numerical calculations of the Z-spectra integrated the differential equations through the continuous-wave sequence using the ordinary differential equation (ODE) solver in *MATLAB* (MathWorks, Natick, MA).

2.8 | Data analysis

All data analyses were performed using *MATLAB* R2018a. All fitting methods for in vivo experiments were performed voxel by voxel with images smoothed by a 3×3 median filter before fitting. The fitting was performed to achieve the lowest RMS of residuals between the data and model. Regions of interest of the stroke lesion were manually outlined from the R_{1obs} map acquired at 1.5-2 hours after the onset of stroke, and applied to all other parametric maps acquired at different time points. Regions of interest of the contralateral normal tissue were chosen to mirror the stroke regions of interest. Student t-tests were used to evaluate differences in parameters, which were considered to be statistically significant when $p < .05$.

3 | RESULTS

3.1 | Quantification of APT and amine CEST effects in ischemic stroke animal models

Figure 1A,C,E, and G shows the average CEST Z-spectra from the stroke lesions and the contralateral normal tissues of five rat brains, respectively, acquired before and 0.5-1 hour, 1-1.5 hours, and 1.5-2 hours after the onset of stroke. Three major CEST dips can be clearly observed at approximately 3.5 ppm, 2 ppm, and −3.5 ppm on the CEST Z-spectra, which have been assigned to APT, arginine amine CEST, and aliphatic NOE, respectively. The NOE(−1.6) peak can also be observed in the contralateral normal tissues but not in the stroke lesions. Figure 1B,D,F, and H shows the corresponding average spectra of the $AREX_{mfit}$ fit of amine CEST, the $AREX_{3pt}$ quantification of APT, and the $AREX_{poly}$ fit of amine CEST from the stroke lesions and the contralateral normal tissues acquired at different time points. It was found that the $AREX_{3pt}$ metric can isolate the APT peak at approximately 3.5 ppm from the background signals, and the $AREX_{poly}$ metric can isolate the arginine amine CEST peak at approximately 2 ppm from the background signals. However, on the $AREX_{mfit}$ fit of the amine CEST spectra, there is a narrow peak at approximately 2 ppm, which is overlaid on a broad sloping baseline.

Figure 2 shows the flipped CEST Z-spectra from the creatine and glutamate samples, respectively. There is a narrow peak from the creatine sample and a broad sloping baseline from the glutamate sample. Compared with the curve from the creatine sample, the broad sloping baseline from the glutamate sample extends to the upfield frequency offsets. This sample experiment suggests that the narrow peak in the brains should be due to the arginine amine, and that the broad sloping baseline in the brains should be due to the fast exchanging pools such as the lysine amines. Thus, the $AREX_{mfit}$ fit of amine CEST at 2 ppm in the brains should have contributions from both the arginine amine pool and the fast exchanging pool, whereas the $AREX_{mfit}$ fit of amine CEST at other
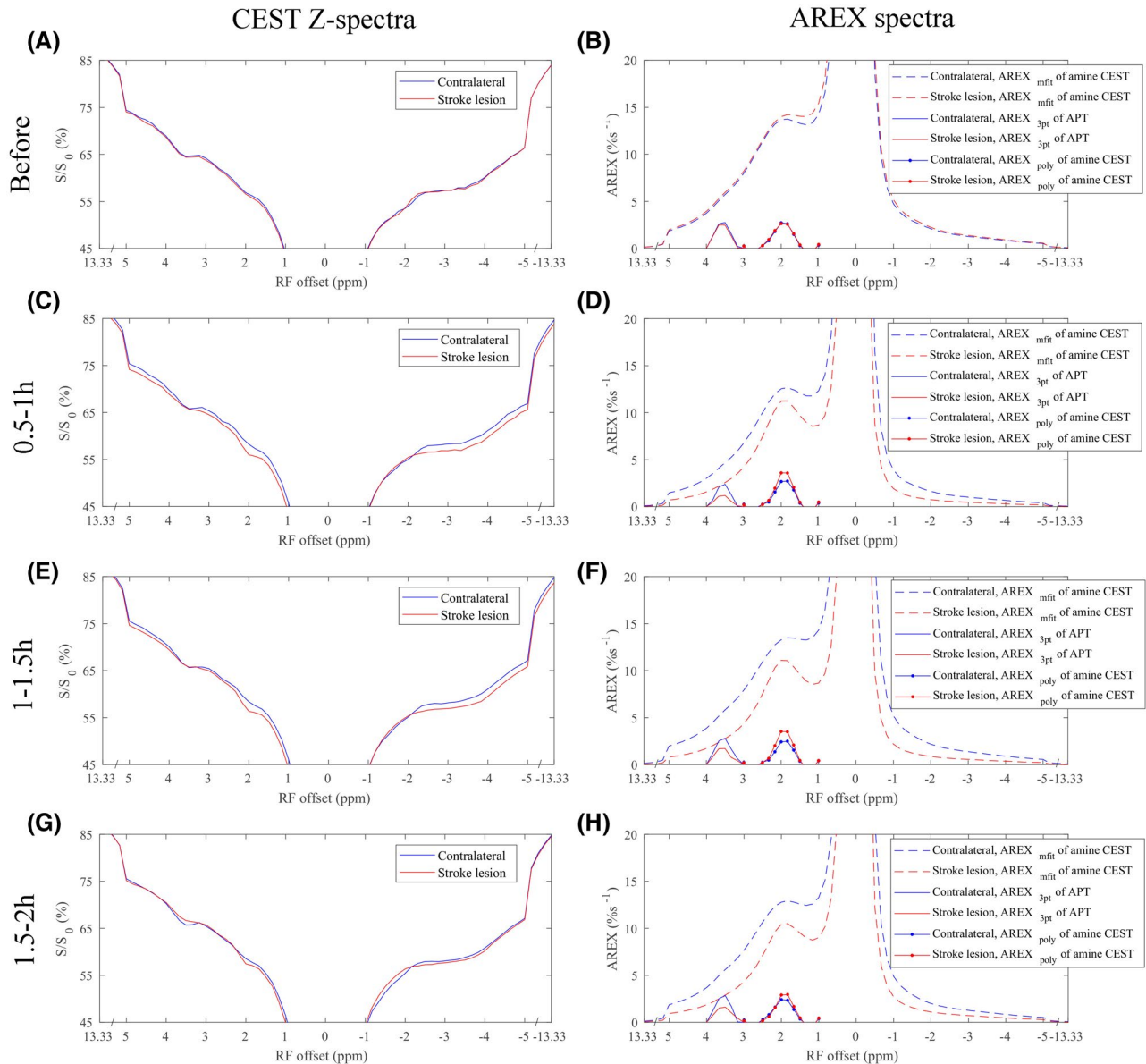
FIGURE 1 Average CEST Z-spectra (left column), spectra of exchange-dependent relaxation multiple-pool Lorentzian lineshape fit (AREX$_{mfit}$) of amine CEST (dashed line), three-point quantification (AREX$_{3pt}$) fit of amide proton transfer (APT; solid line), and polynomial fit (AREX$_{poly}$) of amine CEST (dotted line) (right column) from stroke lesion (red) and contralateral normal tissue (blue) of five rat brains, respectively, acquired before (A,B), 0.5-1 hour (C,D), 1-1.5 hours (E,F), and 1.5-2 hours (G,H) after the onset of stroke

frequency offsets in the brains should have contribution only from the fast exchanging pools. Here, we used the AREX$_{mfit}$ fit of amine CEST at 3 ppm, −2 ppm, and −3 ppm to study the variation in the broad sloping baseline for the stroke lesion.

Figure 3 shows the time-dependent statistics of several AREX metrics from the stroke lesions and the contralateral normal tissues. The AREX$_{3pt}$ quantification of APT at 3.5 ppm in Figure 3A decreased significantly 0.5-1 hour ($p = .008$), 1-1.5 hours ($p = .016$), and 1.5-2 hours ($p = .03$) after the onset of stroke, suggesting that AREX$_{3pt}$ quantification of APT is sensitive in detecting ischemia. In contrast, the AREX$_{poly}$ fit of amine CEST at 2 ppm in Figure

3C increased significantly 1-1.5 hours ($p = .040$) after the onset of the stroke as well as at 0.5-1 hour, although the increase was not significant ($p = .062$). The AREX$_{mfit}$ fit of amine CEST at 2 ppm in Figure 3B decreased significantly at 1-1.5 hour (0.002) and 1.5-2 hours (0.000) after the onset of stroke. The AREX$_{mfit}$ fit of amine CEST at 3 ppm, −2 ppm, and −3 ppm in Figure 2D-F also decrease significantly at 0.5-1 hour ($p = .001, .020,$ and $.026$ for the three offsets), at 1-1.5 hours ($p = .007, .014,$ and $.019$ for the three offsets), and at 1.5-2 hours ($p = .005$ for the offset at 3 ppm), suggesting that the CEST effect from the fast exchanging pools decreased significantly in ischemic stroke. Figure 4 shows the maps of anatomy, R$_{1obs}$, f$_m$, and

FIGURE 2 Flipped CEST Z-spectra $(1-S/S_0)$ from samples of creatine (blue) and glutamate (red) with RF saturation power of 1 μT. The solid arrow indicates the narrow peak from the arginine amine of creatine. The three dashed arrows indicate the broad sloping baseline from the lysine amine of glutamate
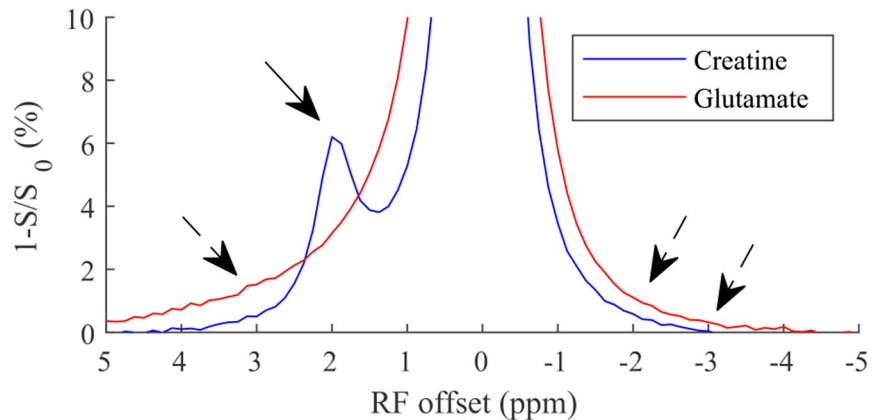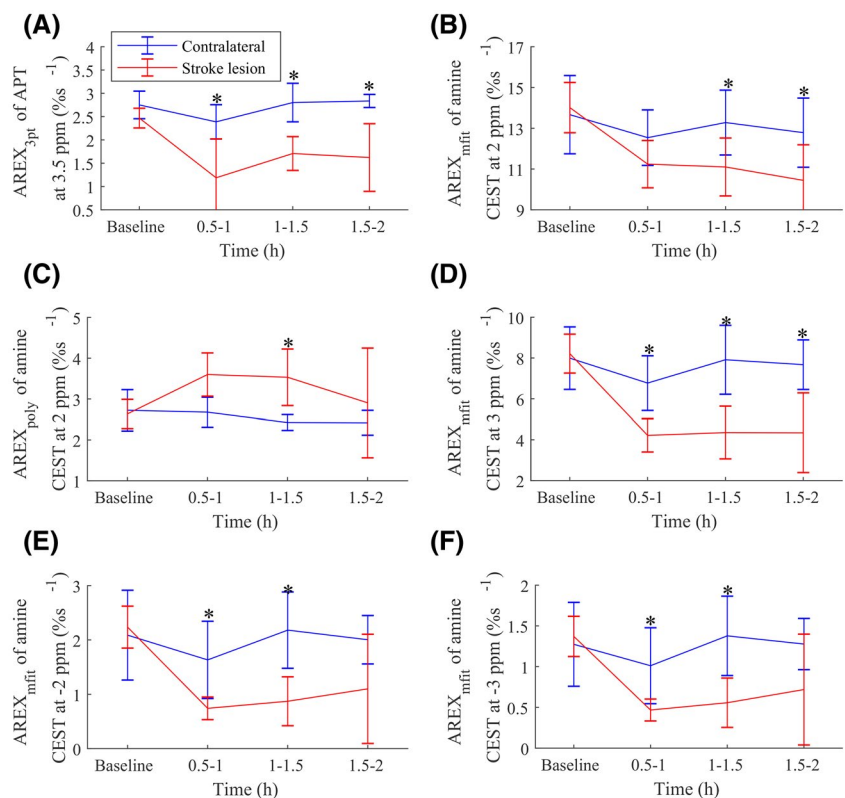

FIGURE 3 Time-dependent statistics of $AREX_{3pt}$ of APT at 3.5 ppm (A), $AREX_{mfit}$ of amine CEST at 2 ppm (B), $AREX_{poly}$ of amine CEST at 2 ppm (C), $AREX_{mfit}$ of amine CEST at 3 ppm (D), $AREX_{mfit}$ of amine CEST at −2 ppm (E), and $AREX_{mfit}$ of amine CEST at −3 ppm (F) in stroke lesion (red) and contralateral normal tissue (blue) (*$p < .05$)

the AREX metrics from a representative rat brain longitudinally after stroke. There were visible changes in R_{1obs} and all AREX parameters after the onset of stroke. Note that the R_{1obs}, $AREX_{3pt}$ fit of APT at 3.5 ppm, $AREX_{mfit}$ fit of amine CEST effect at 2 ppm, and $AREX_{mfit}$ fit of amine CEST effect at 3 ppm had "negative" contrast in the stroke lesion. In contrast, the $AREX_{poly}$ fit of amine at 2 ppm had "positive" contrast in the stroke lesion.

Figure 5 shows the correlations between the $AREX_{3pt}$ quantification of APT at 3.5 ppm and the AREX fit of amine CEST effects. Significant correlations were found for the $AREX_{poly}$ fit of amine CEST effect at 2 ppm ($p = .0008$) and the $AREX_{mfit}$ fit of amine CEST effects at 3 ppm, −2 ppm, and −3 ppm ($p = .0014, .0019$, and $.0022$, respectively) but not for the $AREX_{mfit}$ fit of amine CEST effect at 2 ppm ($p = .5256$). These results suggest that the

change in both the arginine amine and the fast exchanging pools are related to pH. The insignificant correlation between the $AREX_{3pt}$ quantification of APT at 3.5 ppm and the $AREX_{mfit}$ fit of amine CEST effect at 2 ppm could be due to the opposite change of the two CEST effects from the arginine amine and the fast exchanging pools.

3.2 | Simulations and sample studies to show the source of the CEST contrast in stroke lesions

Figure 6 shows the simulated $AREX_{mfit}$ and $AREX_{poly}$ fit of CEST effects versus the solute-water exchange rate (k_{sw}). Note that the $AREX_{poly}$ metric had no contributions from the fast exchanging pools, but the $AREX_{mfit}$

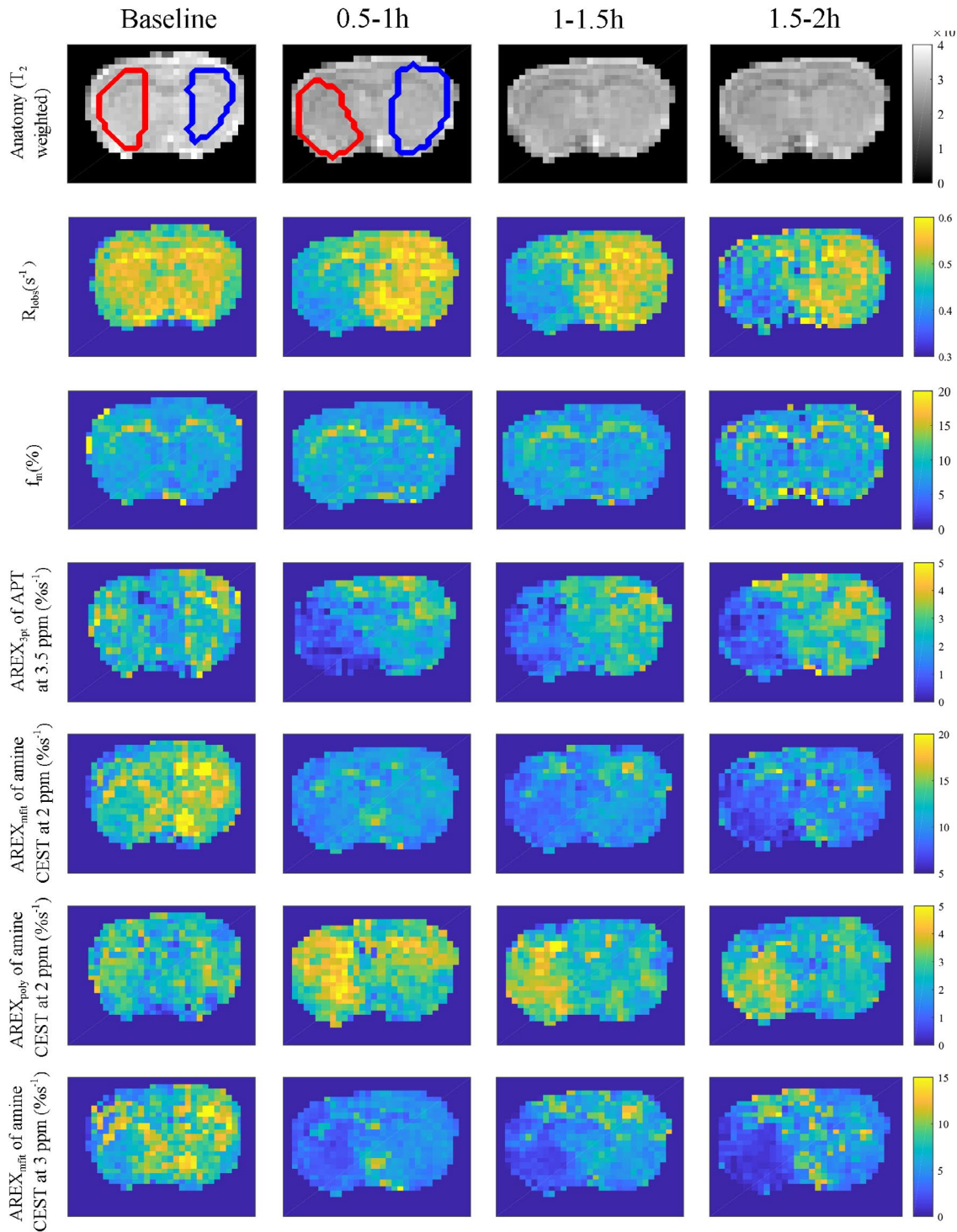**FIGURE 4** Maps of anatomy (T_2-weighted), R_{1obs}, f_m AREX$_{3pt}$ fit of APT at 3.5 ppm, AREX$_{mfit}$ fit of amine CEST at 2 ppm, AREX$_{poly}$ fit of amine CEST at 2 ppm, and AREX$_{mfit}$ fit of amine CEST at 3 ppm acquired at different time points before and after ischemic stroke from a representative rat brain. Regions of interest of lesion (red) and contralateral normal tissue (blue) are shown in the anatomical maps

metric had contributions from the pools in all exchange regimes. This simulation further confirmed that the AREX$_{poly}$ fit of amine CEST can isolate the intermediate exchanging arginine amine pool from the fast exchanging pool, but the AREX$_{mfit}$ fit of amine CEST effect at 2 ppm has contributions from both the arginine amine

and the fast exchanging pools in the animal studies. Additionally, note that both the AREX$_{mfit}$ and the AREX$_{poly}$ fit of CEST signals decreased with increased exchange rate when they were in the intermediate or fast exchanging regimes, suggesting that they should have increased CEST signals in the stroke lesion if the solute

FIGURE 5 Correlations between the AREX$_{3pt}$ fit of APT at 3.5 ppm and AREX$_{mfit}$ of amine CEST at 2 ppm (A), AREX$_{poly}$ of amine CEST at 2 ppm (B), AREX$_{mfit}$ of amine CEST at 3 ppm (C), AREX$_{mfit}$ of amine CEST at −2 ppm (D), and AREX$_{mfit}$ of amine CEST at −3 ppm (E), respectively. The circles represent the mean values of each ROI from stroke lesion acquired at different time points after onset of stroke. Spearman's rank correlation coefficient (r) and *p*-value of the correlation are provided. The solid line represents the linear regression of all data points
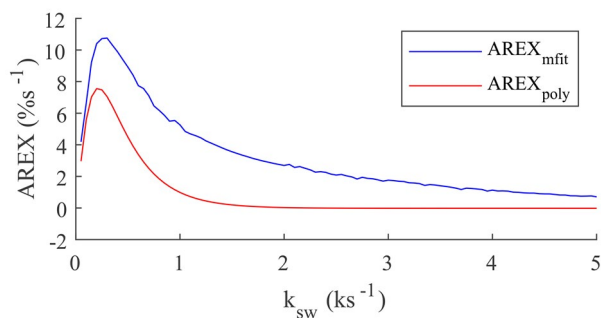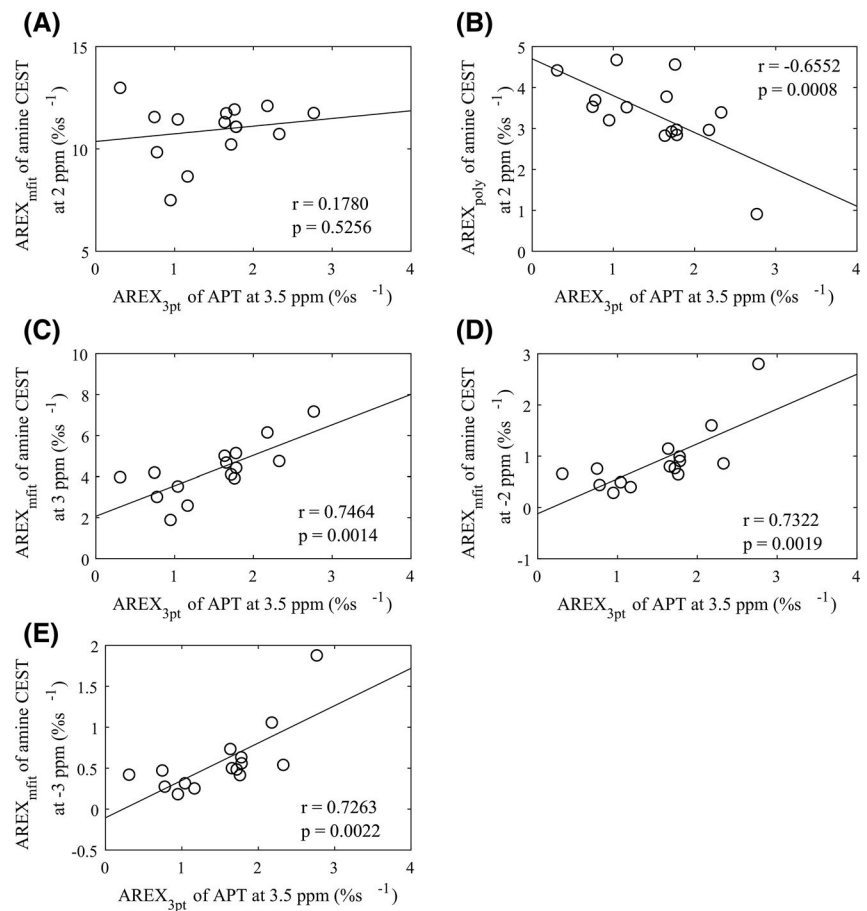
FIGURE 6 Two-pool model simulated AREX$_{mfit}$ and AREX$_{poly}$ versus k$_{sw}$

concentration did not change. Figure 7 shows the measured CEST Z-spectra and the corresponding AREX spectra on two samples of tissue homogenates with different pH values. Note that the AREX$_{poly}$ fit of amine CEST at 2 ppm, as well as the narrow peak and the broad sloping baseline on the AREX$_{mfit}$ spectra, increase with decreasing pH, confirming the simulations. The results from the simulations and sample studies are in agreement with the increased AREX$_{poly}$ fit of amine at 2 ppm and the bigger narrow peak on the spectra of the AREX$_{mfit}$ fit of amine CEST effect in the stroke lesion, but not with

the decreased baseline on the spectra of the AREX$_{mfit}$ fit of amine CEST. A possible explanation could be the decreased solute concentration, which may be due to the decreased content of metabolites with fast exchanging protons or edema after stroke.

4 | DISCUSSION

A significant CEST effect from phosphocreatine at approximately 2.6 ppm has been previously reported in muscle.[19,30,31] In the brain, the decrease in the AREX$_{mfit}$ fit of amine CEST at 3 ppm might also be due to the reduced phosphocreatine in ischemia. However, phosphocreatine is in the slow to intermediate exchange regime[32]; thus, its CEST peak cannot extend to the up-field frequency offsets. In our experiments, we found that the AREX$_{mfit}$ fit of amine CEST at 3 ppm, −2 ppm, and −3 ppm for all time points (0.5-2 hours) decreased from 7.45% ± 1.32% to 4.30% ± 1.42%, from 1.94% ± 0.63% to 0.90% ± 0.62%, and from 1.22% ± 0.43% to 0.58% ± 0.42%, respectively, suggesting that the change in the sloping baseline should be primarily due to the change in the fast exchanging pool. In the fast exchanging regime and with the use of low RF saturation powers, the increase in the AREX$_{mfit}$ fit of the
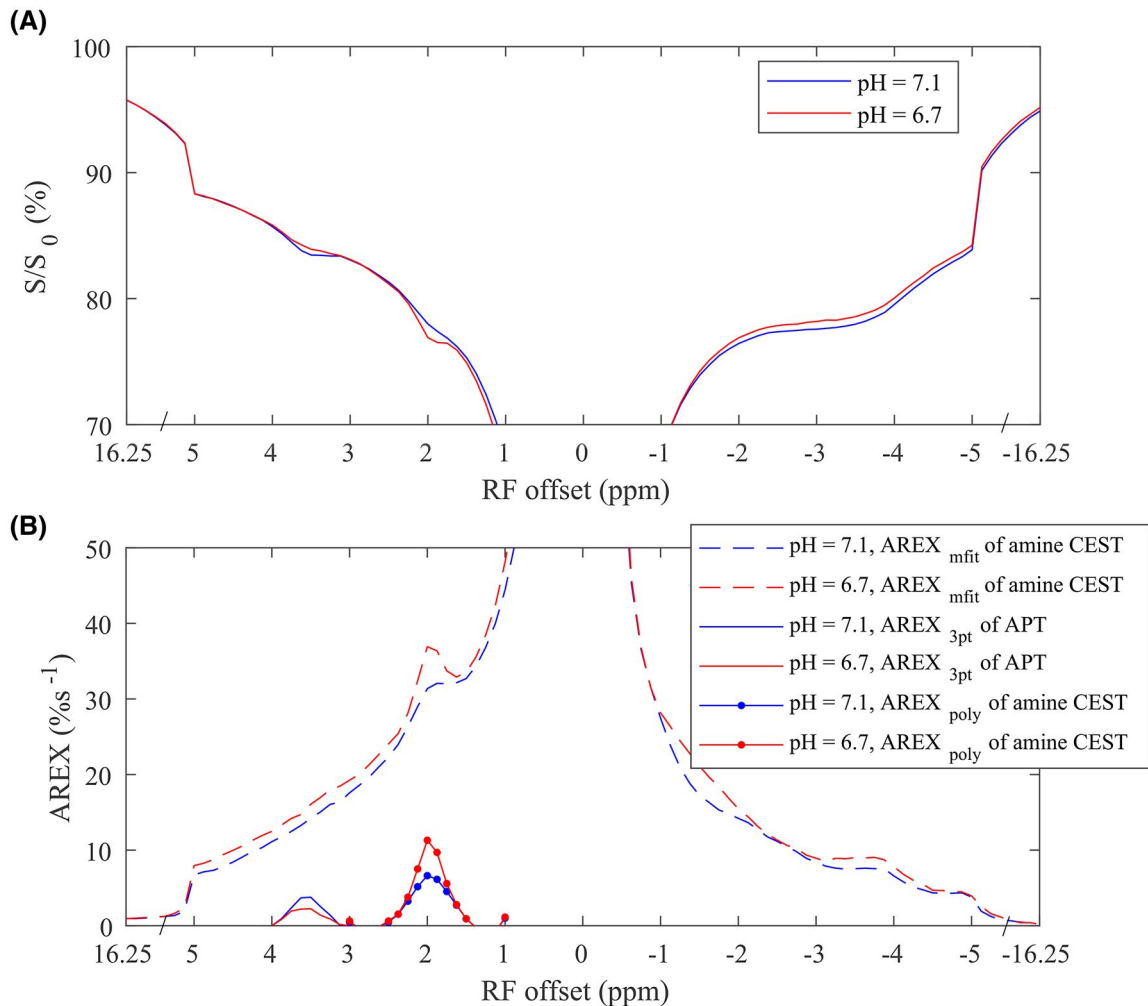
(A)

(B)

FIGURE 7 The CEST Z-spectra (A) and corresponding spectra of $AREX_{mfit}$ fit of amine CEST, $AREX_{3pt}$ fit of APT, and $AREX_{poly}$ fit of amine CEST (Bs) from two samples of tissue homogenates with pH of 6.7 (red) and 7.1 (blue), respectively

amine CEST effect due to the reduced exchange rate is relatively small, as shown in Figure 6. Thus, our animal studies suggest that the concentration of the fast exchanging pool in vivo should decrease by at least half. The contribution from fast exchanging pools to CEST signals acquired at relatively low RF saturation powers cannot be clearly observed on the CEST Z-spectrum due to the broad peak as shown in Figure 1, and thus has been overlooked previously. However, our study suggests that it is noticeable, changes significantly in stroke lesions, and influences the multiple-pool Lorentzian lineshape fit of the arginine amine CEST effect at 2 ppm.

The relative contribution from the intermediate exchanging arginine amine and the fast exchanging pools depends on the RF saturation power and B_0 field. In the current study and our previous study[15] at 7 T as well as Wu et al at 4.7 T,[14] the contribution to CEST signals from the change in the fast exchanging pool may be greater than or comparable to that from the change in the arginine amine pool, leading to a significantly reduced or unchanged

multiple-pool Lorentzian fitted amine CEST effect at 2 ppm in the stroke lesion. In contrast, in Tee et al[17] at 9.4 T, the fast exchanging pool may be relatively far from 2 ppm, and thus has weaker contribution at 2 ppm, leading to a significantly increased amine CEST effect at 2 ppm in the stroke lesion. In a recent study, Zhou et al[24] performed a seven-pool (amide, amine at 2.75 ppm, amine at 2 ppm, water, NOE[−1.6], NOE[−3.5], and semisolid MT) model fit of CEST signals from global ischemia acquired with ω_1 of 0.75 μT at 4.7T MRI, and found that the fitted amine CEST effect at 2.75 ppm decreased significantly, but the fitted amine CEST effect at 2 ppm increased significantly in global ischemia. In this seven-pool model fit, the pool of amine at 2.75 ppm may model the fast exchanging pool, which increased the accuracy in fitting the arginine amine at 2 ppm. This previous study and our analysis suggest that an additional pool representing the fast exchanging amine may be added to the multiple-pool Lorentzian fit to increase the accuracy in quantifying arginine amine at 2 ppm.

Although the $AREX_{poly}$ fit of amine CEST at 2 ppm has a strong correlation with the $AREX_{3pt}$ quantification of APT at 3.5 ppm, there was a significant difference between the stroke lesions and the contralateral normal tissues 1-1.5 hours after the onset of the stroke only. This may be due to the large SD across subjects that arises from the nonrobustness of this fitting method. The polynomial fit may overestimate or underestimate the amine CEST effect, depending on the reference signal and the order of the polynomial coefficients. For the fitting of CEST signals acquired on the same animal but at different time points after stroke, the fitting errors may be close; thus, the fitted values can still reflect the variation of the CEST effect. However, for the fitting of CEST signals acquired from different animals, the fitting errors may be different, resulting in large SD across subjects.

The two red dots at 1 ppm and 3 ppm in Figure 1B,D,F, and H as well as in Figure 7B are due to the errors in the polynomial fit of amine CEST at 2 ppm. Thus, optimization of the reference sampling points and/or the order of the polynomial fit to increase the fitting robustness are required in future studies. Also, optimization of sequence parameters to enhance the contribution from the intermediate exchanging arginine amine pool in the multiple-pool Lorentzian fit is required. New sequences for specific quantification of arginine amine CEST at 2 ppm can also improve the CEST pH imaging of ischemic stroke. For example, we have developed a chemical exchange rotation transfer technique that can isolate the slow and intermediate exchanging pools from the fast exchanging pools. Previously, we applied this technique to specifically quantify the arginine amine CEST effect at 2 ppm in brain tumors.[33] Future studies may evaluate its application in detecting ischemic stroke.

The molecular origin of the fast exchanging pool that contributes to the decreased CEST effect in stroke is not clear. The strong correlations between the $AREX_{3pt}$ quantification of APT and the $AREX_{mfit}$ fit of amine CEST effects at 3 ppm, −2 ppm, and −3 ppm in Figure 5C-E suggest that the fast exchanging pool that changes in ischemia may be related to anaerobic metabolism. Previously, we showed that both glutamate and proteins contain fast exchanging protons that contribute to CEST effect at 3 ppm.[9] However, several publications[8,34,35] reported increased glutamate concentration in stroke. Edema could also lead to a reduced concentration of metabolites. However, our fitted M_{0w} values were $(5.5 \times 10^4 \pm 1.6 \times 10^3, 5.5 \times 10^4 \pm 0.3 \times 10^3)$, $(5.5 \times 10^4 \pm 1.9 \times 10^3, 5.5 \times 10^4 \pm 0.7 \times 10^3)$, and $(5.5 \times 10^4 \pm 1.8 \times 10^3, 5.5 \times 10^4 \pm 0.6 \times 10^3)$ in the stroke lesions and contralateral normal tissues 0.5-1 hour, 1-1.5 hours, and 1.5-22 hours after onset of the stroke, respectively, suggesting that edema could not contribute to the reduced concentration of the fast exchanging pool in our study. Future studies evaluating the contrast origin of the fast exchanging pool are warranted and may lead to a new pH or molecular imaging biomarker for detecting ischemic stroke.

One limitation of the current study is that we used a specific set of saturation parameters. When other saturation parameters are used, the relative contributions from the arginine amine and the fast exchanging pools could be different, and some of our observations, such as the correlation between APT and amine CEST effects, might change. Another limitation is the accuracy of the fitting methods, which depends on the saturation parameters and the sampling points. Our previous study has evaluated the accuracy of the three-point quantification of APT and found that it underestimates the APT signal.[21] The CEST signal at around 2.6 ppm, which has been assigned to be phosphocreatine,[19,30,31,36] may influence the reference signal for the polynomial fit. This CEST dip at around 2.6 ppm can be observed in the Z-spectra from contralateral normal tissues in Figure 1C,E. These quantification errors may also influence the correlations between APT and amine CEST effects. In this study, we assumed that the AREX metric can specifically quantify the CEST effects. However, if it is influenced by the variation in T_{1w}, the decreased baseline on the spectra of the $AREX_{mfit}$ fit of amine CEST from the stroke lesion could be explained by the decreased concentration of fast exchanging pool and/or the increased T_{1w}.

5 | CONCLUSIONS

This paper suggests that fast exchanging pools contribute to the CEST signals acquired at relatively low RF saturation power, which has been overlooked previously, and could greatly influence the quantification of the arginine amine CEST effect. The multiple-pool Lorentzian fit of amine CEST effect at 2 ppm has contributions from both the arginine amine and the fast exchanging pools, which change in the opposite direction during ischemic stroke, leading to an insignificant correlation of the Lorentzian fit of amine CEST effects with APT and the different results in different experimental conditions reported previously. The polynomial fit of amine CEST effect at 2 ppm can isolate arginine amine from the fast exchanging pool, and thus has a strong correlation with the APT imaging in stroke.

ORCID

Jing Cui https://orcid.org/0000-0003-0902-8715
Zhongliang Zu https://orcid.org/0000-0001-7361-7480

REFERENCES

1. Zhou JY, van Zijl PCM. Defining an acidosis-based ischemic penumbra from pH-weighted MRI. *Trans Stroke Res*. 2012;3:76-83.

2. Sun PZ, Zhou JY, Sun WY, Huang J, van Zijl PCM. Detection of the ischemic penumbra using pH-weighted MRI. *J Cereb Blood Flow Metab*. 2007;27:1129-1136.

3. van Zijl PCM, Zhou J, Mori N, Payen JF, Wilson D, Mori S. Mechanism of magnetization transfer during on-resonance water saturation. A new approach to detect mobile proteins, peptides, and lipids. *Magn Reson Med*. 2003;49:440-449.

4. Zhou JY, Payen JF, Wilson DA, Traystman RJ, van Zijl PCM. Using the amide proton signals of intracellular proteins and peptides to detect pH effects in MRI. *Nat Med*. 2003;9:1085-1090.

5. Sun PZ, Cheung JS, Wang EF, Lo EH. Association between pH-weighted endogenous amide proton chemical exchange saturation transfer MRI and tissue lactic acidosis during acute ischemic stroke. *J Cerebr Blood F Met*. 2011;31:1743-1750.

6. Zhang XY, Xie JP, Wang F, et al. Assignment of the molecular origins of CEST signals at 2 ppm in rat brain. *Magn Reson Med*. 2017;78:881-887.

7. Chen L, Zeng HF, Xu X, et al. Investigation of the contribution of total creatine to the CEST Z-spectrum of brain using a knock-out mouse model. *NMR Biomed*. 2017;30:e3834.

8. Cai KJ, Haris M, Singh A, et al. Magnetic resonance imaging of glutamate. *Nat Med*. 2012;18:302-306.

9. Cui J, Zu ZL. Towards the molecular origin of glutamate CEST (GluCEST) imaging in rat brain. *Magn Reson Med*. 2020;83:1405-1417.

10. Cai KJ, Singh A, Poptani H, et al. CEST signal at 2 ppm (CEST@2ppm) from Z-spectral fitting correlates with creatine distribution in brain tumor. *NMR Biomed*. 2015;28:1-8.

11. Haris M, Singh A, Cai KJ, et al. A technique for in vivo mapping of myocardial creatine kinase metabolism. *Nat Med*. 2014;20:209-214.

12. Rerich E, Zaiss M, Korzowski A, Ladd ME, Bachert P. Relaxation-compensated CEST-MRI at 7T for mapping of creatine content and pH—preliminary application in human muscle tissue in vivo. *NMR Biomed*. 2015;28:1402-1412.

13. Kogan F, Haris M, Singh A, et al. Method for high-resolution imaging of creatine in vivo using chemical exchange saturation transfer. *Magn Reson Med*. 2014;71:164-172.

14. Wu Y, Zhou IY, Lu DS, et al. pH-sensitive amide proton transfer effect dominates the magnetization transfer asymmetry contrast during acute ischemiaquantification of multipool contribution to in vivo CEST MRI. *Magn Reson Med*. 2018;79:1602-1608.

15. Zhang XY, Wang F, Afzal A, et al. A new NOE-mediated MT signal at around −1.6 ppm for detecting ischemic stroke in rat brain. *Magn Reson Imaging*. 2016;34:1100-1106.

16. Jin T, Wang P, Hitchens TK, Kim SG. Enhancing sensitivity of pH-weighted MRI with combination of amide and guanidyl CEST. *Neuroimage*. 2017;157:341-350.

17. Tee YK, Abidin B, Khrapitcheve A, et al. CEST and NOE signals in ischemic stroke at 9.4T evaluated using a Lorentzian multi-pool analysis: a drop, an increase or no change? In: Proceedings of the 25th Annual Meeting of ISMRM, Honolulu, Hawaii, 2017. p 3782.

18. Zong XP, Wang P, Kim SG, Jin T. Sensitivity and source of amine-proton exchange and amide-proton transfer magnetic resonance imaging in cerebral ischemia. *Magn Reson Med*. 2014;71:118-132.

19. Chen L, Barker PB, Weiss RG, van Zijl PCM, Xu JD. Creatine and phosphocreatine mapping of mouse skeletal muscle by a polynomial and Lorentzian line-shape fitting CEST method. *Magn Reson Med*. 2019;81:69-78.

20. Hua J, Jones CK, Blakeley J, Smith SA, van Zijl PCM, Zhou JY. Quantitative description of the asymmetry in magnetization transfer effects around the water resonance in the human brain. *Magn Reson Med*. 2007;58:786-793.

21. Zhang XY, Wang F, Li H, et al. Accuracy in the quantification of chemical exchange saturation transfer (CEST) and relayed nuclear Overhauser enhancement (rNOE) saturation transfer effects. *NMR Biomed*. 2017;30:e3716.

22. Jin T, Wang P, Zong XP, Kim SG. MR imaging of the amide-proton transfer effect and the pH-insensitive nuclear Overhauser effect at 9.4 T. *Magn Reson Med*. 2013;69:760-770.

23. Xu JZ, Zaiss M, Zu ZL, et al. On the origins of chemical exchange saturation transfer (CEST) contrast in tumors at 9.4 T. *NMR Biomed*. 2014;27:406-416.

24. Zhou IY, Lu DS, Ji Y, et al. Determination of multipool contributions to endogenous amide proton transfer effects in global ischemia with high spectral resolution in vivo chemical exchange saturation transfer MRI. *Magn Reson Med*. 2019;81:645-652.

25. Zu ZL. Ratiometric NOE(-1.6) contrast in brain tumors. *NMR Biomed*. 2018;31:e4017.

26. Windschuh J, Zaiss M, Meissner JE, et al. Correction of B1-inhomogeneities for relaxation-compensated CEST imaging at 7T. *NMR Biomed*. 2015;28:529-537.

27. Zaiss M, Zu ZL, Xu JZ, et al. A combined analytical solution for chemical exchange saturation transfer and semi-solid magnetization transfer. *NMR Biomed*. 2015;28:217-230.

28. Zaiss M, Xu JZ, Goerke S, et al. Inverse Z-spectrum analysis for spillover-, MT-, and T1-corrected steady-state pulsed CEST-MRI—application to pH-weighted MRI of acute stroke. *NMR Biomed*. 2014;27:240-252.

29. Gochberg DF, Gore JC. Quantitative magnetization transfer imaging via selective inversion recovery with short repetition times. *Magn Reson Med*. 2007;57:437-441.

30. Chen L, Schär M, Chan KWY, et al. In vivo imaging of phosphocreatine with artificial neural networks. *Nat Commun*. 2020;11:1072.

31. Zu ZL, Lin EC, Louie EA, et al. Chemical exchange rotation transfer imaging of phosphocreatine in muscle. *NMR Biomed*. 2021;34:e4437.

32. Haris M, Nanga RPR, Singh A, et al. Exchange rates of creatine kinase metabolites: feasibility of imaging creatine by chemical exchange saturation transfer MRI. *NMR Biomed*. 2012;25:1305-1309.

33. Zu ZL, Louie EA, Lin EC, et al. Chemical exchange rotation transfer imaging of intermediate-exchanging amines at 2 ppm. *NMR Biomed*. 2017;30:e3756.

34. Davalos A, Shuaib A, Wahlgren NG. Neurotransmitters and pathophysiology of stroke: evidence for the release of glutamate and other transmitters/mediators in animals and humans. *J Stroke Cerebrovasc Dis*. 2000;9:2-8.

35. Kiewert C, Mdzinarishvili A, Hartmann J, Bickel U, Klein J. Metabolic and transmitter changes in core and penumbra after middle cerebral artery occlusion in mice. *Brain Res.* 2010;1312:101-107.

36. Chung JJ, Jin T, Lee JH, Kim SG. Chemical exchange saturation transfer imaging of phosphocreatine in the muscle. *Magn Reson Med.* 2019;81:3476-3487.

SUPPORTING INFORMATION

Additional supporting information may be found in the online version of the article at the publisher's website.

FIGURE S1 Averaged CEST Z-spectrum (black) and the corresponding polynomial function fitted spectra with different orders from contralateral normal tissue (A) and stroke lesion (B) of 5 rat brains. Note that the polynomial fit with order of 3 can fit the background CEST signals from 3-2.5 ppm and 1.5-1 ppm with sufficient accuracy